Available online at www.sciencedirect.com
SCIENCE DIRECT
Geochimica et Cosmochimica Acta 70 (2006) 2325–2336
Geochimica
www.elsevier.com/locate/gca

Pb diffusion in monazite: An experimental study of $Pb^{2+} + Th^{4+} \Longleftrightarrow 2Nd^{3+}$ interdiffusion

Emmanuel Gardés [a,*], Olivier Jaoul [a,†], Jean-Marc Montel [a], Anne-Magali Seydoux-Guillaume [a], Richard Wirth [b]

[a] *Laboratoire des Mécanismes et Transferts en Géologie, 14 avenue Edouard Belin, 31400 Toulouse, France*
[b] *GeoForschungsZentrum-Potsdam, Telegrafenberg, 14473 Potsdam, Germany*

Received 8 July 2005; accepted in revised form 23 January 2006

Abstract

We have measured Pb diffusivity in synthetic $NdPO_4$ crystals from an epitaxial $Nd_{0.66}Pb_{0.17}Th_{0.17}PO_4$ thin film deposited on (−1 0 1) faces. Annealings were performed at room pressure at temperatures ranging from 1200 to 1500 °C for 1 h to 1 month. Samples were analysed using transmission electron microscopy (TEM) and Rutherford backscattering spectrometry (RBS). TEM demonstrates that Pb and Th diffuse together from the thin film towards the crystal and Nd in the opposite direction, according to the interdiffusion exchange $Pb^{2+} + Th^{4+} \Longleftrightarrow 2Nd^{3+}$. RBS was used to perform depth profiling of all samples. Measured diffusivities follow the Arrhenius law:

$$\log D_0(\mathrm{m^2\ s^{-1}}) = -3.41 \pm 0.77,$$

$$E = 509 \pm 24\ \mathrm{kJ\ mol^{-1}}.$$

The extrapolation of these data to crustal temperatures yield very low diffusivities. For instance, the time necessary for a 50 μm grain to lose all of its Pb at 800 °C is calculated to be greater than the age of the Earth. From these results and other evidence from the literature, we conclude that most of the perturbations in U–Th–Pb ages of monazite cannot be attributed to Pb diffusion, but rather to interactions with fluids.

1. Introduction

In any geochronological system, the significance of the measured age depends on the way the radiometric system is reset. A geochronological system can be disturbed by gain or loss of radioactive elements and their decay products. For monazite, which after zircon is the most widely used mineral in U–Th–Pb dating (Parrish, 1990; Harrison et al., 2002), the age perturbations are mainly attributed to Pb deficiencies. However the mechanisms by which Pb is lost are not fully constrained. Contrary to zircon, monazite is rarely metamict and enhanced Pb loss due to the amorphization of the lattice is improbable (Meldrum et al., 1998; Seydoux-Guillaume et al., 2004). Monazites often display discrete age domains attributed to interactions with fluids during metamorphic events (e.g., DeWolf et al., 1993; Bingen and van Breemen, 1998; Braun et al., 1998; Cocherie et al., 1998; Crowley and Ghent, 1999; Zhu and O'Nions, 1999; Seydoux-Guillaume et al., 2003; Paquette et al., 2004). Indeed, experimental studies under hydrothermal conditions (Teufel and Heinrich, 1997; Seydoux-Guillaume et al., 2002) indicate that dissolution–reprecipitation is an efficient mechanism to disturb the U–Pb monazite ages.

Although it is well known that recrystallization mediated by fluids is a viable mechanism for Pb loss in monazite, it is important to investigate whether or not Pb

* Corresponding author.
E-mail address: egardes@lmtg.obs-mip.fr (E. Gardés).
† Pr. Olivier Jaoul made a strong contribution to this work, but unfortunately died on November 15, 2005.

0016-7037/$ - see front matter © 2006 Elsevier Inc. All rights reserved.
doi:10.1016/j.gca.2006.01.018

diffusion can also disturb the monazite U–Th–Pb ages. Diffusion data can thus be used to constrain apparent age interpretations via quantification of Pb loss during thermal events and closure temperature calculations (Dodson, 1973; Ganguly and Tirone, 1999). Suzuki et al. (1994) reported >10 μm Pb concentration profiles in metamorphic monazites. Assuming these profiles were induced by diffusion, they estimated a diffusion law with Arrhenius parameters $\log D_0(m^2\,s^{-1}) = -10.47$ (−15.07 to 3.34) and $E = 244$ (118 to 529) kJ mol^{-1}. Experimental measurements of Pb diffusivity have been performed by Smith and Giletti (1997) and Cherniak et al. (2004) who, respectively, found Arrhenius parameters $\log D_0(m^2\,s^{-1}) = -14.18 \pm 1.54$ and $E = 180 \pm 48$ kJ mol^{-1}, and $\log D_0(m^2\,s^{-1}) = -0.03 \pm 1.35$ and $E = 594 \pm 39$ kJ mol^{-1}. Extrapolations from Suzuki et al. (1994), Smith and Giletti (1997) and Cherniak et al. (2004) data at 700 °C, for a 100 Ma duration, yield characteristic diffusion lengths ($2\sqrt{Dt}$) of about 200, 100, and 0.01 μm, respectively. While the results of Suzuki et al. (1994) and Smith and Giletti (1997) are in close agreement and indicate that Pb loss via diffusion can occur at reasonable metamorphic temperatures, they differ drastically from the results of Cherniak et al. (2004), which prohibits significant diffusion up to extreme temperatures for crust.

Even though no study reports measurements of the oxidation state of Pb in natural monazite, the temperature–oxygen fugacity conditions in common geological settings are reducing and thus incompatible with the Pb^{4+} state. Similar to Pb-brabantite $Pb_{0.5}Th_{0.5}PO_4$ (isostructural with monazite), Pb should be divalent in natural monazite. Therefore, Pb diffusion via $Pb^{2+} \Longleftrightarrow LREE^{3+}$ exchange is unlikely since at least one other species should be involved to maintain electroneutrality, a feature which has not been taken into account in the previous experimental studies. In order to add new constraints on Pb diffusivity in monazite, we carried out $Pb^{2+} + Th^{4+} \Longleftrightarrow 2Nd^{3+}$ interdiffusion experiments between $Nd_{0.66}Pb_{0.17}Th_{0.17}PO_4$ monazite thin films and synthetic $NdPO_4$ monazite crystals. As Th is a major element in monazite, it should be a good candidate for charge compensation. Diffusion profiles were analysed with transmission electron microscopy (TEM), using the recent focused ion beam (FIB) sample preparation technique, and the more conventional RBS technique.

2. Experimental procedure

2.1. Sample preparation

$NdPO_4$ and $Nd_{0.66}Pb_{0.17}Th_{0.17}PO_4$ powders were synthesized using a sol–gel method (adapted from Montel et al., 2002). Nd_2O_3 was dissolved in a HNO_3 solution and H_3PO_4 was added in stoichiometric proportion. A gel was obtained by lowering the pH by addition of variable amounts of NH_4OH. The gel was rinsed, dried at 80 °C, and then ground and calcined in air at 1200 °C overnight to evaporate water and nitrogen compounds and also to crystallize $NdPO_4$ with the monazite structure. For $Nd_{0.66}Pb_{0.17}Th_{0.17}PO_4$ we used the same procedure but PbO and $Th(NO_3)_4$ were added to the nitric acid solution before precipitating the gel. After each synthesis, the crystallinity of the powders was checked by X-ray diffraction and the chemical composition by electron microprobe.

Large $NdPO_4$ monazite crystals were made using a flux-growth technique (e.g., Boatner, 2002). $NdPO_4$ powder was mixed with the flux in a 5:95 weight ratio. The mixture was loaded in a platinum crucible and heated at 1300 °C in air overnight to completely dissolve the $NdPO_4$ powder in the melted flux. The temperature was then linearly lowered to ~900 °C for durations ranging from ~3 days to ~3 weeks. We tried three different fluxes: WO_3–Li_2WO_4 in a 44:56 weight ratio, PbO–$(NH_4)_2HPO_4$ in a 62:38 weight ratio and MoO_3–$Na_2MoO_4.2H_2O$ in a 48:52 weight ratio. After growth, the crystals were collected by dissolving the flux in boiling solutions of KOH, HNO_3, and H_2O, respectively. In these three cases, the crystals were pink, plate-shaped, and up to more than 1 mm in width and several hundred micrometers in thickness (Fig. 1). X-Ray crystal diffraction showed that the larger faces of the crystals are (−1 0 1). Table 1 gives the electron microprobe analysis for three crystals synthesized with the three different fluxes. There is no evidence of dissolved flux in the crystals from the W- and Mo-based fluxes, although some of these crystals exhibit inclusions that should contain flux (not analysed). However, crystals grown in Pb-based flux contain ~1 wt% PbO as found by Donovan et al. (2003). For diffusion experiments we selected crystals with large (−1 0 1) faces (about 1 mm^2) and no cracks or inclusions. The (−1 0 1) crystal faces were polished down to 1 μm with diamond lapping films, then with 0.02 μm colloidal silica. The polished surfaces were subsequently chemically etched with a ~50 wt% H_2SO_4 solution for a few tens of seconds and pre-annealed in air at 1400 °C overnight. The diffusant thin film was deposited on the (−1 0 1) faces of the $NdPO_4$ crystals by radio-frequency sputtering of the $Nd_{0.66}Pb_{0.17}Th_{0.17}PO_4$ powder. To measure the thin film thicknesses, Si wafers were placed near the samples and analysed using a Dektak mechanical step profiler after each sputtering run. The thin films were ~50–150 nm thick, depending on the sputtering duration and the position of the samples in the apparatus.

2.2. Diffusion experiments

The samples were annealed in Al_2O_3 tubes using a horizontal furnace with $LaCrO_3$ heating elements. Temperature was controlled using a Pt/Pt-10%Rh thermocouple close to the samples (<5 mm). With these settings, the maximum temperature uncertainty is ±5 °C. The samples were enclosed in welded ~4 mm diameter and ~8 mm long Pt capsules filled with ~4 mm diameter $Nd_{0.66}Pb_{0.17}Th_{0.17}PO_4$ sintered-powder pellets that act as a Pb buffer. The capsules were designed so that the pellets did not touch the samples.

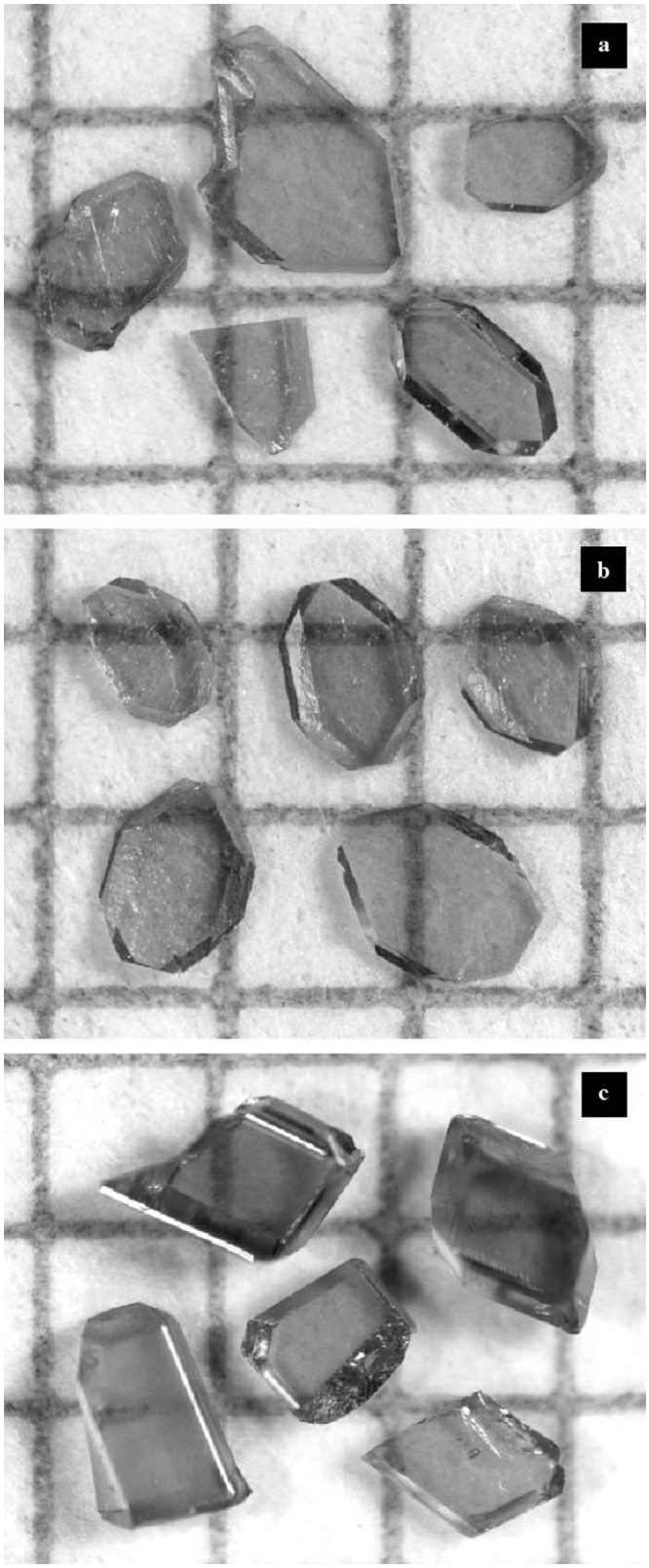

Fig. 1. $NdPO_4$ crystals synthesized with (a) W-, (b) Pb- and (c) Mo-based fluxes (1 mm × 1 mm grid). The large plated faces are (−1 0 1).

This assembly plays a crucial role for controlling the stoichiometry of the thin films during annealings, especially the Th/Pb ratio. Electron microprobe analyses of thin films from samples annealed in air without the Pb buffer revealed high Th/Pb ratios, indicating that strong evaporation of Pb had occurred. With the $Nd_{0.66}Pb_{0.17}Th_{0.17}PO_4$ pellets, Pb evaporation is buffered, producing in most cases thin films with Th/Pb ratios less than two. The thin film composition was checked using electron microprobe after each run, and all samples with Th/Pb ratios greater than two were rejected. The thin film surfaces of the annealed samples are continuous and smooth. A topography study using a Zygo 3-D optical profiler indicates that the average film thickness variation was less than 10%. Thus the thin films are in continuous contact over the samples, with little deviation in thickness.

Table 1
Electron microprobe phase composition and structural formula for three $NdPO_4$ crystals synthesized with W-, Pb- and Mo-based fluxes (Cameca SX50, EMPA facility at the Université Paul Sabatier, Toulouse)

	W	Pb	Mo
P_2O_5	29.9	28.9	29.6
Nd_2O_3	69.9	70.8	70.8
MoO_3	—	—	<0.1
Na_2O	—	—	<0.1
PbO	—	1.0	—
WO_3	<0.1	—	—
Total	99.8	100.7	100.5
P	1.00	0.98	1.00
Nd	0.99	1.01	1.01
Mo	—	—	<0.01
Na	—	—	<0.01
Pb	—	0.02	—
W	<0.01	—	—

Oxides are in wt%. The structural formulas are calculated on a 4-oxygen basis.

3. Results

3.1. Transmission electron microscopy

We used the recent Focused gallium Ion Beam (FIB) technique (FEI FIB200 instrument at the GeoForschungs-Zentrum-Potsdam) which allows cutting electron transparent foils (∼15 μm × 8 μm × 0.1 μm) perpendicular to the surface of a solid (Overwijk et al., 1993; Young, 1997; Roberts et al., 2001; Wirth, 2004). This technique produces constant thickness foils, which are very suitable for the acquisition of line scans or elemental maps with TEM (Seydoux-Guillaume et al., 2003; Wirth, 2004). TEM investigations were performed at the GeoForschungsZentrum-Potsdam with a Philips CM200 device equipped with a LaB_6 filament operating at 200 kV. We used convergent beam electron diffraction (CBED) to investigate the crystallographic structure of the diffusion zone by focusing the beam with a spot size of ∼40 nm. The TEM is equipped with an energy dispersive X-ray analyzer (EDAX) with an ultrathin window. As the instrument was not calibrated with standards, only relative abundances were measured

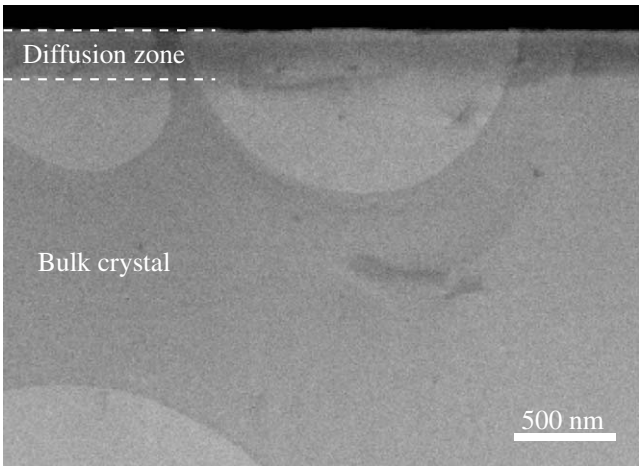

Fig. 2. TEM bright field image of the foil cut perpendicular to sample Nd1M1-5 surface (annealed at 1400 °C for 9.50×10^4 s). The diffusion zone is darker than the bulk crystal because the absorption of Pb and Th is greater than that of Nd. No major structural defects can be observed in the thin film. The diffusion front is planar, as expected for 1-D diffusion. The brighter rounded areas represent holes in the carbon membrane of the TEM copper grid on which the foil is mounted.

along linear traverses using Pb (Mα), Th (Mα), and Nd (Lα) X-ray intensities.

FIB–TEM foils were cut perpendicular to the diffusion surface of samples Nd5M8-32, Nd1M1-5, and Nd1M1-19 (annealed at 1400 °C for 8.00×10^3 s, at 1400 °C for 9.50×10^4 s and at 1500 °C for 7.96×10^4 s, respectively). Fig. 2 is a bright field image of the foil cut in sample Nd1M1-5. No major structural defects can be observed in the thin film and the diffusion front is planar. The CBED investigations revealed that both the crystal core and the diffusion zone have similar lattice parameters and orientation. This implies that the thin film is epitaxially crystallized on the crystal. Pb, Th, and Nd profiles obtained along one linear traverse for sample Nd1M1-5 foil are presented in Fig. 3. This figure shows that Pb and Th diffuse from the thin film towards the crystal, whereas Nd diffuses from the crystal towards the thin film. In order to determine the diffusivities, we fitted each profile with the 1-D solution to the diffusion equation for a diffusant layer of thickness h deposited on a semi-infinite substrate (Crank, 1975):

$$C(x,t) = \left(\frac{C_0 - C_\infty}{2}\right) \times \left(\operatorname{erf}\left(\frac{x+h}{2\sqrt{Dt}}\right) - \operatorname{erf}\left(\frac{x-h}{2\sqrt{Dt}}\right)\right) + C_\infty, \quad (1)$$

where the x-axis is perpendicular to the diffusion interface, the diffusant reservoir lies between $x = 0$ and $x = h$ and the substrate is at $x > h$. C_0 is the initial layer concentration and C_∞ the initial concentration in the substrate. This solution assumes the diffusivity D is independent of concentration. As illustrated in Fig. 3, Pb, Th, and Nd experimental profiles can be fit using this solution. Thus, no strong dependence of the diffusivities on concentration is found. The extracted diffusivities from TEM profiles are reported

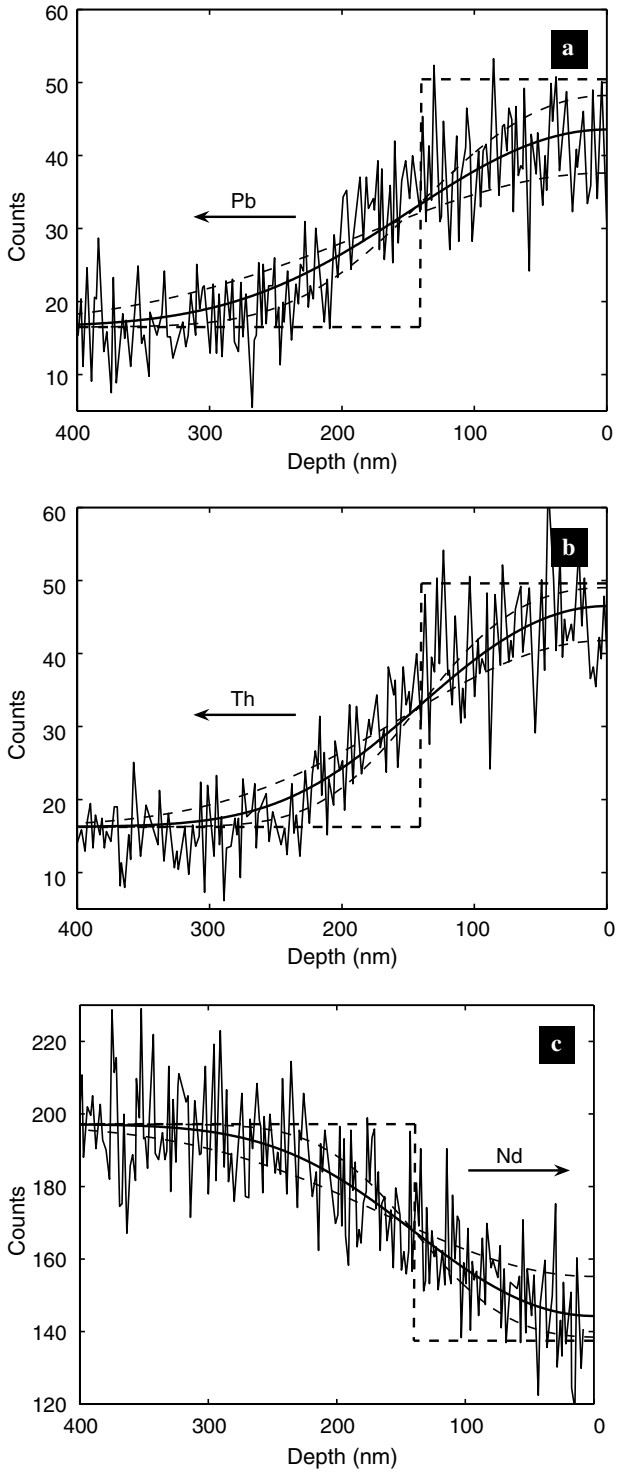

Fig. 3. (a) Pb, (b) Th, and (c) Nd TEM-EDAX profiles obtained in the diffusion zone of sample Nd1M1-5 (annealed at 1400 °C for 9.50×10^4 s) along linear traverse 3 (see Table 2). The surface of the sample is on the right of the plots (at depth "0") and the core is on the left. These three plots illustrate the diffusion of Pb and Th from the thin film towards the crystal and the diffusion of Nd from the crystal towards the thin film. The initial profiles (straight dashed lines) are shown, the step representing the initial interface between the thin film and crystal. The raw intensity profiles (noisy solid lines) were adjusted using least-squares fits (smooth solid lines) with the solution of diffusion equation [Eq. (1)], assuming concentrations proportional to intensities. The $+2\sigma$ and -2σ simulated profiles are also shown (thin smooth dashed lines).

Table 2
Diffusivities extracted from TEM-EDAX profiles (given as $\log D$, with D in $m^2\ s^{-1}$)

Traverse	Pb	Th	Nd	All
	Nd5M8-32 (1400 °C − 8.00×10^3 s)			
1	-19.28 ± 0.88	-19.16 ± 0.87	-19.20 ± 0.48	
2	-19.10 ± 0.88	-19.08 ± 0.87	-18.65 ± 0.48	
3	-18.78 ± 0.88	-18.79 ± 0.87	-18.84 ± 0.48	
4	-19.45 ± 0.88	-19.49 ± 0.87	-18.89 ± 0.48	
5	-19.97 ± 0.88	-19.93 ± 0.87	-19.20 ± 0.48	
Average	-19.32 ± 0.40	-19.29 ± 0.39	-18.96 ± 0.21	-19.19 ± 0.20
	Nd1M1-5 (1400 °C − 9.50×10^4 s)			
1	-19.07 ± 0.32	-19.11 ± 0.30	-19.05 ± 0.36	
2	-19.49 ± 0.32	-19.25 ± 0.30	-19.11 ± 0.36	
3	-19.19 ± 0.32	-19.43 ± 0.30	-19.39 ± 0.36	
4	-19.27 ± 0.32	-19.44 ± 0.30	—	
5	-19.35 ± 0.32	-19.36 ± 0.30	—	
6	-19.30 ± 0.32	-19.28 ± 0.30	—	
7	-19.44 ± 0.32	-19.60 ± 0.30	—	
8	-19.60 ± 0.32	-19.60 ± 0.30	—	
9	-19.44 ± 0.32	-19.47 ± 0.30	—	
10	-19.46 ± 0.32	-19.29 ± 0.30	—	
11	-19.16 ± 0.32	-19.28 ± 0.30	—	
Average	-19.34 ± 0.10	-19.37 ± 0.09	-19.18 ± 0.21	-19.34 ± 0.07
	Nd1M1-19 (1500 °C − 7.96×10^4 s)			
1	-18.77 ± 0.35	-18.83 ± 0.48	—	
2	-18.79 ± 0.35	-18.63 ± 0.48	-18.53 ± 1.05	
3	-18.55 ± 0.35	-18.73 ± 0.48	-18.64 ± 1.05	
4	-18.98 ± 0.35	-19.18 ± 0.48	-19.49 ± 1.05	
Average	-18.77 ± 0.18	-18.84 ± 0.24	-18.89 ± 0.53	-18.83 ± 0.17

For each sample, Pb, Th, and Nd profiles yield similar diffusivities, as expected for $Pb^{2+} + Th^{4+} \Longleftrightarrow 2Nd^{3+}$ exchange. The "All" column reports the average diffusivities over all species profiles for each sample.

in Table 2. For each sample, no significant differences can be found between the diffusivities extracted from Pb, Th, and Nd profiles. The Pb and Th profiles are identical and the Nd profile is complementary. Thus, these three species diffuse at the same rate, which is the interdiffusion coefficient D for the exchange $Pb^{2+} + Th^{4+} \Longleftrightarrow 2Nd^{3+}$.

3.2. Rutherford backscattering spectrometry

Rutherford backscattering spectrometry (RBS) is an appropriate technique for investigating the first few micrometers under a solid surface (e.g., Feldman and Mayer, 1986) and is commonly used for diffusion studies in the Earth sciences (e.g., Jaoul et al., 1991). We carried out RBS analyses with the Van de Graaff accelerator at the Institut des NanoSciences de Paris using a 2 MeV α-particles beam of ~0.5 mm diameter. Samples were exposed to ~30–50 nA beam current for a few minutes so that the charge was 5 or 10 μC. This produced enough backscattered particles to attain good counting statistics. Backscattered particles were detected using a Si surface barrier detector (2 msr solid angle), placed at 165° with respect to the beam direction. The overall detector and electronic resolution of the system was ~20 keV (FWHM), which is equivalent in our samples to ~20 nm depth resolution for Pb, Th, and Nd. RBS spectra were modelled and diffusion coefficients were extracted with RUMP program (Doolittle, 1985, 1986) using the solution of diffusion equation [Eq. (1)]. Despite the power of the RBS technique, we had to solve two problems. First, the high mass elements are in a narrow band of energy on the RBS spectra. Due to interdiffusion, Pb, Th, and Nd signals are present in the energy channels of each of these three species. These overlaps make the precise differentiation of Pb, Th, and Nd profiles difficult. However, given the TEM results, we modelled all RBS spectra with identical diffusion rates for Pb, Th and Nd. A second problem is that RBS analysis on crystallized materials can be disturbed by channeling (Cohen, 1972; Feldman and Mayer, 1986). When aligned with the main crystallographic directions, the impinging particles may be channeled along crystal rows or planes and the interactions with the crystal nuclei are reduced. Channeling modifies the shape of the RBS spectra causing an over- or under-estimation of the diffusion coefficients. The best way to avoid channeling is to run analyses in various directions approximately normal to the crystal surface in order to find a non-channeling direction, called "random" (L'Hoir et al., 1981). However, this procedure is complex and time consuming and should be repeated on each sample. As we had several tens of samples to analyse, we set up a simplified procedure. We acquired series of spectra with the sample tilted at different arbitrary small angles (<~3°). Most of the time, because of channeling,

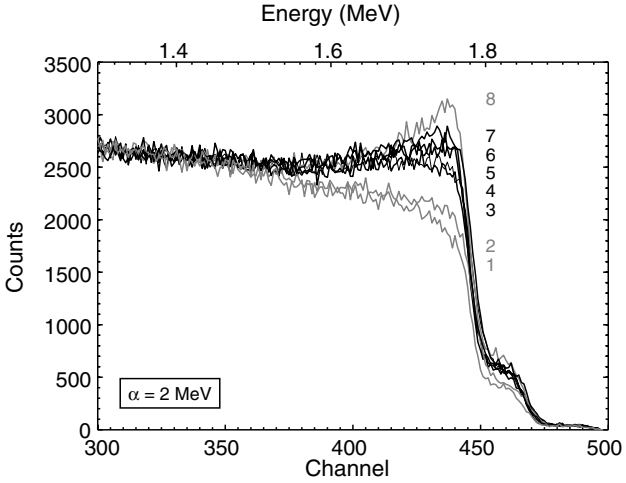

Fig. 4. RBS spectra of sample Nd1M1-19 (annealed at 1500 °C for 7.96×10^4 s). The eight spectra were taken with the sample tilted at eight different angles (<~3°) about the beam. The grey spectra (1, 2, and 8) are strongly channeled. They cannot be modelled using RUMP and were not considered. In spectra 1 and 2, the surface atoms are under-counted which would result in an over-estimation of the diffusion coefficients if modelled. Conversely, the fit of spectrum 8 would result in an under-estimation of the diffusion coefficient. The black spectra (3, 4, 5, 6, and 7) are close to each other but there are still slight discrepancies due to weak channeling. These five spectra were selected to extract five diffusion coefficients ($\log D(m^2\ s^{-1}) = -18.40$, -18.40, -18.66, -18.50, and -18.61 for spectra 3, 4, 5, 6, and 7, respectively) and to calculate the average diffusivity in this sample ($\log D(m^2\ s^{-1}) = -18.51$).

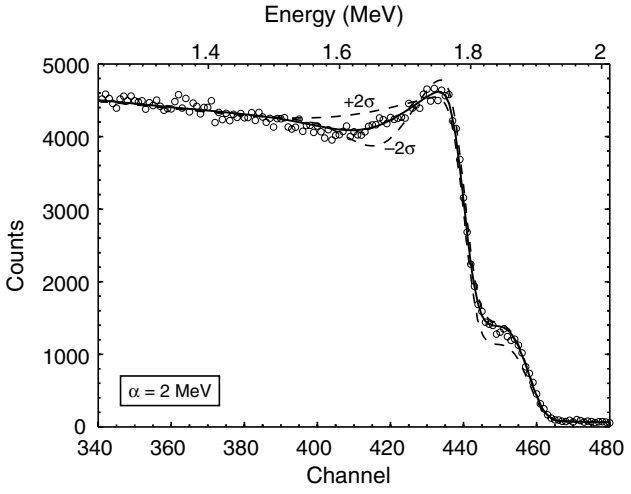

Fig. 5. Experimental RBS spectrum (circles) on sample Nd1M1-5 (annealed at 1400 °C for 9.50×10^4 s), modelled using RUMP (solid and dashed lines).

spectra have different shapes for each beam direction. Strongly channeled spectra are easy to detect (Fig. 4) and cannot be modelled with RUMP. These spectra were systematically rejected. The other spectra can be modelled with RUMP but their shape may slightly differ from each other, due to weak channeling (Fig. 4). These spectra were selected. As the deviations on extracted diffusivities due to weak channeling can be positive or negative, we assumed they are randomly distributed and that reliable diffusion coefficients can be obtained by averaging.

RBS analyses made on unannealed samples never showed evidence for channeling. Conversely, channeling often occurred on annealed samples. An investigation on sample Nd4M5-47 (annealed at 1350 °C for 2.67×10^5 s) showed that when the beam was aligned with $[-101]^*$, channeling was as intense as channeling in uncoated $NdPO_4$ crystals. In addition, spectra of samples annealed only a few minutes at temperatures around 1200 °C also exhibit channeling. We conclude that: (1) the thin film is amorphous after the radio-frequency sputtering coating procedure; (2) the thin film is epitaxially crystallized on the crystal after annealing, as found with TEM; and (3) crystallization of the thin film occurs during the earliest stages of the annealings.

One of the RBS spectra acquired on sample Nd1M1-5 (annealed at 1400 °C for 9.50×10^4 s) is shown in Fig. 5. For this sample, the average diffusivity calculated from the RBS data ($\log D(\mathrm{m^2\,s^{-1}}) = -19.68 \pm 0.35$) is compatible with the TEM value ($\log D(\mathrm{m^2\,s^{-1}}) = -19.34 \pm 0.07$). This is also true for the other two samples investigated with TEM (Nd5M8-32 and Nd1M1-19). These results show that TEM and RBS are in agreement. Consequently, the simplified RBS procedure used in this study is reliable and does not introduce significant bias. On 48 samples, more than 200 RBS spectra were acquired. About 25% of them were strongly channeled and rejected. Only two samples were rejected because diffusion lengths were too small ($2\sqrt{Dt} \sim 20$ nm) compared to the RBS resolution. The diffusion lengths of the other samples ranged from ~30 to ~300 nm. Table 3 presents the average diffusivities extracted from RBS spectra for each sample. Examination of the data reveals that: (1) the diffusion coefficients are independent of the annealing durations (Fig. 6a), (2) the

Table 3
Average diffusivities for $Pb^{2+} + Th^{4+} \Longleftrightarrow 2Nd^{3+}$ interdiffusion in $NdPO_4$ normal to (−101), as obtained from RBS

Sample	T (°C)	Time (s)	$\log D(\mathrm{m^2\,s^{-1}})$	Number[a]	Flux[b]	Th/Pb[c]
Nd5M8-31	1200	2.67×10^6	-22.01 ± 0.25	6/1	Mo	1.50
Nd5M9-11	1200	2.67×10^6	-21.30 ± 0.27	5/2	Mo	1.62
Nd5M9-22	1200	2.67×10^6	-21.61 ± 0.23	7/4	Mo	1.05
Nd5M9-23	1200	2.67×10^6	-21.43 ± 0.27	5/2	Mo	1.64
Nd5M9-18	1250	6.55×10^5	-21.04 ± 0.30	4/3	Mo	1.46
Nd5M9-19	1250	6.55×10^5	-20.70 ± 0.25	6/1	Mo	1.52
Nd5M9-10	1250	1.34×10^6	-20.95 ± 0.30	4/3	Mo	1.51
Nd5M9-20	1250	1.34×10^6	-20.76 ± 0.35	3/4	Mo	1.57
Nd5M9-21	1250	1.34×10^6	-21.10 ± 0.27	5/2	Mo	1.65
Nd5M8-14	1300	1.08×10^5	-20.22 ± 0.43	2/0	Mo	1.18
Nd5M8-15	1300	1.08×10^5	-20.50 ± 0.61	1/0	Mo	1.69
Nd5M8-16	1300	1.08×10^5	-20.66 ± 0.61	1/0	Mo	1.42
Nd4M5-9	1300	1.12×10^5	-20.38 ± 0.43	2/0	Pb	1.17
Nd5M8-18	1300	2.60×10^5	-20.21 ± 0.43	2/1	Mo	1.35
Nd5M9-4	1300	2.60×10^5	-19.78 ± 0.43	2/1	Mo	1.42
Nd5M8-34	1300	3.60×10^5	-20.54 ± 0.30	4/0	Mo	1.10
Nd4M5-3	1300	4.77×10^5	-20.70 ± 0.43	2/0	Pb	1.43
Nd4M5-43	1350	9.12×10^4	-19.26 ± 0.30	4/0	Pb	1.65
Nd4M5-51	1350	9.12×10^4	-19.40 ± 0.25	6/0	Pb	1.3
Nd4M5-47	1350	2.67×10^5	-19.61 ± 0.23	7/2	Pb	1.94
Nd1M1′-1	1350	5.74×10^5	-19.57 ± 0.25	6/1	Pb	1.36
Nd4M5-45	1350	5.74×10^5	-19.43 ± 0.23	7/0	Pb	1.35
Nd4M5-49	1350	5.74×10^5	-19.56 ± 0.25	6/2	Pb	1.86
Nd4M5-21	1400	5.12×10^3	-19.04 ± 0.27	5/0	Pb	1.24
Nd5M8-32	1400	8.00×10^3	-18.79 ± 0.61	1/0	Mo	1.28
Nd4M5-1	1400	1.57×10^4	-19.56 ± 0.43	2/0	Pb	1.17
Nd1M1-5	1400	9.50×10^4	-19.68 ± 0.35	3/3	W	1.03
Nd4M5-15	1400	2.37×10^5	-19.27 ± 0.35	3/2	Pb	1.90
Nd4M5-25	1400	2.37×10^5	-19.17 ± 0.61	1/0	Pb	1.90
Nd4M5-29	1400	2.37×10^5	-19.41 ± 0.61	1/0	Pb	1.33
Nd4M5-35	1400	2.37×10^5	-19.08 ± 0.23	7/2	Pb	1.30
Nd1M1-14B	1400	3.71×10^5	-19.30 ± 0.43	2/5	W	1.28
Nd4M5-36	1400	3.71×10^5	-19.59 ± 0.27	5/0	Pb	1.50
Nd5M8-38	1500	3.35×10^3	-18.42 ± 0.61	1/0	Mo	1.58
Nd5M8-39	1500	3.35×10^3	-18.50 ± 0.61	1/0	Mo	1.75
Nd5M8-40	1500	3.35×10^3	-18.56 ± 0.61	1/0	Mo	1.84
Nd1M1′-3	1500	7.72×10^3	-18.40 ± 0.30	4/1	Pb	1.40
Nd4M5-17	1500	7.72×10^3	-18.24 ± 0.43	2/2	Pb	1.15
Nd4M5-26	1500	7.72×10^3	-18.40 ± 0.61	1/3	Pb	1.22
Nd5M8-35	1500	1.18×10^4	-19.08 ± 0.61	1/0	Mo	1.87
Nd1M1-13	1500	3.28×10^4	-18.49 ± 0.30	4/1	W	1.20
Nd4M5-27	1500	3.28×10^4	-18.67 ± 0.30	4/2	Pb	1.50
Nd4M5-31	1500	3.28×10^4	-18.55 ± 0.25	6/0	Pb	1.10
Nd1M1-19	1500	7.96×10^4	-18.51 ± 0.27	5/3	W	0.96
Nd4M5-32	1500	7.96×10^4	-18.61 ± 0.27	5/1	Pb	1.21
Nd5M9-3	1500	8.02×10^4	-19.37 ± 0.61	1/0	Mo	1.71

[a] Number of selected spectra (weakly channeled, used to calculate the average diffusivity)/number of rejected spectra (strongly channeled).
[b] Flux used for crystal synthesis.
[c] Th/Pb ratio of the thin film after annealing.

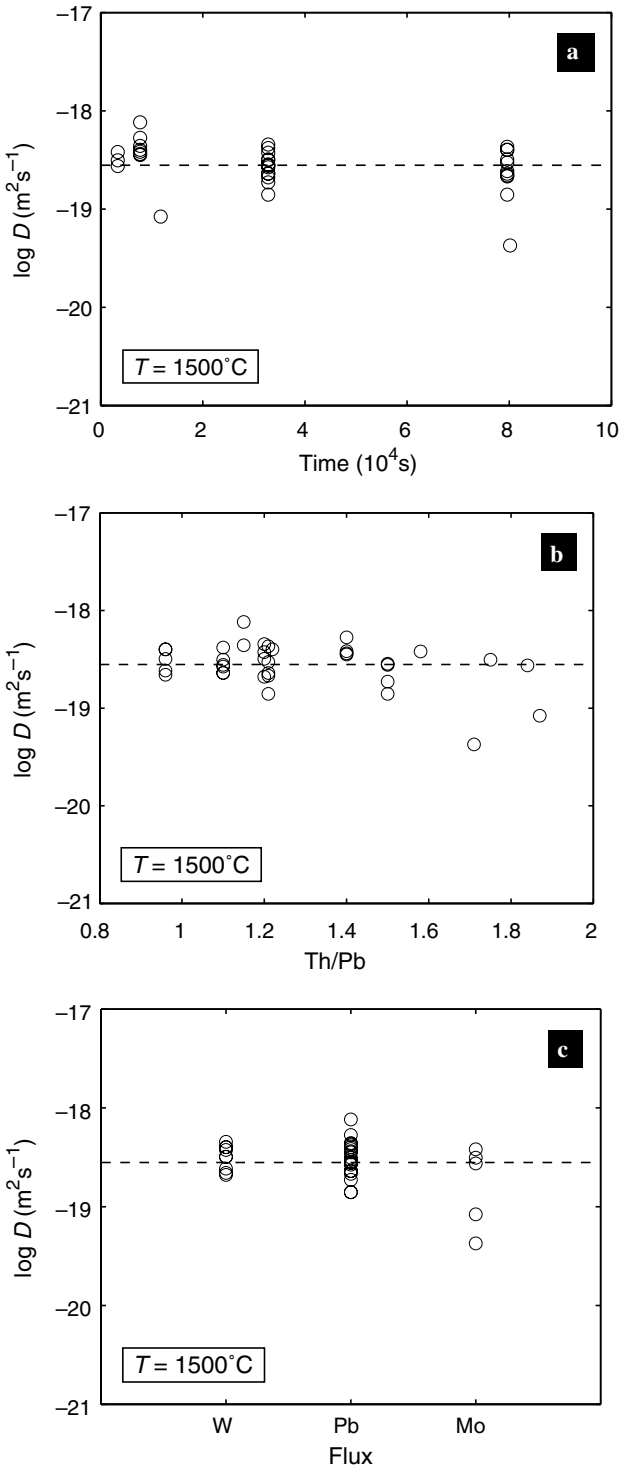

Fig. 6. Plots of diffusivities versus (a) annealing durations, (b) Th/Pb thin film ratios after annealing and (c) fluxes used to synthesized $NdPO_4$ crystals. The data presented here are all the diffusion coefficients obtained by RBS on samples annealed at 1500 °C. There is no significant correlation between the diffusion coefficients and these parameters.

diffusion coefficients do not depend on the Th/Pb ratio of the thin films (Fig. 6b), and (3) the nature of the flux used to synthesize the crystals does not influence the diffusivities (Fig. 6c), even for the crystals synthesized with the Pb-based flux.

An Arrhenius plot of all the RBS data (i.e. all the diffusion coefficients extracted on all samples) is given in Fig. 7. The linear least-squares fit of these data yields an activation energy $E = 509 \pm 24$ kJ mol^{-1} and a pre-exponential factor $\log D_0(\mathrm{m^2\,s^{-1}}) = -3.41 \pm 0.77$.

3.3. Uncertainties

The calculation of uncertainties on diffusivities requires that the uncertainties on all the other parameters are known. However, for both TEM and RBS profiling unknown uncertainties remain, thus the simple propagation of counting errors lead to underestimated uncertainties on diffusivities. Thus we used the variability of the diffusivities over repeated measurements (i.e., the reproducibility) to provide an estimate of the overall uncertainties. In the case of TEM, unknown uncertainty is mainly due to a possible drift in foil position relative to the beam, but this is not likely to be more than ~30 nm. Extracted diffusivities were first regrouped by element (Pb, Th, and Nd) in order to detect eventual discrepancies between the apparent diffusivities of each element. For a given element, the uncertainty on the diffusivity extracted from a single profile has been taken equal to the standard deviation of the diffusivities extrated from all profiles (Table 2). This value is divided by the square root of the number of profiles to obtain the uncertainty on the mean diffusivity for each element (SDOM). Finally, the overall mean and uncertainty on sample (considering all elements) has been calculated using the weighted average and associated standard deviation formula. For RBS, the deviation on extracted diffusivities due to channeling cannot be determined a priori. As channeling is the major contribution to error and should affect

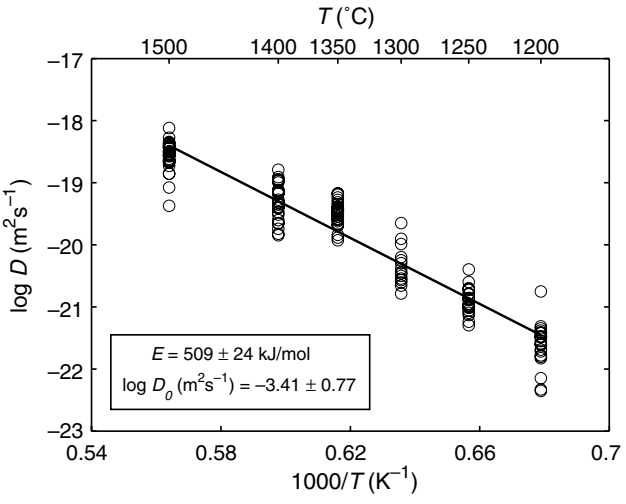

Fig. 7. Arrhenius plot of RBS data for $Pb^{2+} + Th^{4+} \Longleftrightarrow 2Nd^{3+}$ interdiffusion in $NdPO_4$ normal to (−101). It represents all the diffusion coefficients extracted from all samples. Despite the wide scatter of the data, the linear correlation coefficient is good ($r = -0.96$ for these 163 data points). The line is the least-squares fit of the data. It yields an activation energy $E = 509 \pm 24$ kJ mol^{-1} and a pre-exponential factor $\log D_0(\mathrm{m^2\,s^{-1}}) = -3.41 \pm 0.77$.

all samples almost equally, the uncertainty on each single measurement has been taken equal to the standard deviation of the residuals (RMSE) of the Arrhenius fit (Fig. 7). The uncertainty on the sample mean is the SDOM. The 2σ uncertainty ($2 \times$ RMSE) on a single RBS measurement is 0.61 (on $\log D$). This high value is mainly due to the simplified RBS procedure used in this study which introduces noise through weak channeling effects. Nevertheless, the repetition of the measurements (163 RBS data) yields good accuracy on the Arrhenius parameters. The uncertainties reported for the results of the present study are 2σ.

4. Discussion

4.1. What have we measured ?

The thin films are in continuous contact on the crystal surfaces, with little variation in thickness, precluding lateral diffusion. The epitaxial crystallization of the thin film on the crystal substrate allows us to consider the assembly thin film + crystal as a quasi-monocrystal. The accommodation of the thin film lattice on the crystal is possible because $Nd_{0.66}Pb_{0.17}Th_{0.17}PO_4$ and $NdPO_4$ have very close cell parameters (Ni et al., 1995; Montel et al., 2002). Investigations of the thin film using both TEM and RBS demonstrate that no major structural defects occur, which could have modified the diffusivity. This conclusion is confirmed by the planar shape of the diffusion front (Fig. 2). Thus, our experiments are restricted to volume diffusion.

As Pb, Th, and Nd profiles can be fitted with the solution of the diffusion equation used here (Eq. (1)) for both TEM and RBS data, no strong dependence can be found among diffusivity and concentration. This is corroborated by the independence of diffusivities from annealing durations, i.e., for different mean concentrations. This is most probably the consequence of the relatively low initial concentrations of Pb and Th in the thin film, which result in low concentration and activity coefficient gradients.

The Pt capsules we used to enclose the samples were not sealed under vacuum. Consequently, the oxygen fugacity in the capsule atmosphere should be similar to that of air. Considering the oxygen fugacity of air, in the temperature range of our annealings and in the pure Pb–O system, Pb is divalent. Even if our assemblage is more complex, there is no reason to suspect a significant presence of Pb^{4+} in the thin film, as suggested by the fact that Pb-brabantite can be synthesized in air at high temperature.

The only diffusion direction investigated was $[-101]^*$. However, the diffusion anisotropy found by Smith and Giletti (1997) is low (2–5 times slower parallel to *c*-axis) and was not observed by Cherniak et al. (2004). Thus, diffusion anisotropy should not be important and the unique direction investigated here should be comparable to all the other directions within one order of magnitude.

The co-diffusion of Pb^{2+} and Th^{4+} observed in these experiments is induced by the ionic coupling among these two species, since their fluxes must be equal in order to maintain electroneutrality. The diffusion of the ion pair is then controlled by the diffusion of the slower cation. Considering that activation energy is proportional and mainly related to site energy (Dowty, 1980), Th^{4+} diffusion should be more sluggish than that of Pb^{2+}, as Th^{4+} charge is greater than that of Pb^{2+}. However the radius of Pb^{2+}, 1.35 Å, is much greater than the radius of Th^{4+}, 1.09 Å (ninefold coordination; Shannon, 1976). As ionic porosity is low in monazite (Dahl, 1997), cationic radius may play an important role in the diffusivities. In this case, Pb^{2+} diffusion would be more sluggish than Th^{4+} diffusion. Thus, based on these considerations, it is not possible to draw an a priori conclusion on the relative diffusivities of Pb and Th.

4.2. Comparison with previous experimental studies

Smith and Giletti (1997) performed experiments on natural monazites with an enriched ^{204}Pb salt evaporated onto the surface of the samples. They analysed their diffusion profiles using SIMS and found an Arrhenius law with parameters $\log D_0(m^2\,s^{-1}) = -14.18 \pm 1.54$ and $E = 180 \pm 48$ kJ mol^{-1}. Cherniak et al. (2004) worked on synthetic $CePO_4$ and natural monazite, using RBS and SIMS analysis, performing in- and out-diffusion experiments. The Arrhenius parameters from RBS data they obtained by inward diffusion of a $CePO_4$–$PbZrO_3$ powder diffusant source into synthetic $CePO_4$ are $\log D_0(m^2\,s^{-1}) = -0.03 \pm 1.35$ and $E = 594 \pm 39$ kJ mol^{-1}. Our values, $\log D_0(m^2\,s^{-1}) = -3.41 \pm 0.77$ and $E = 509 \pm 24$ kJ mol^{-1}, are close to those of Cherniak et al. (2004), especially the activation energy (Fig. 8). At 700 °C, for a 100 Ma duration, our data yield a small characteristic length of diffusion of ~0.05 μm, in close agreement with the Cherniak et al. (2004) data (~0.01 μm).

The only common experimental temperature between this study and that of Smith and Giletti (1997) is 1200 °C. At this temperature our average diffusivity is one order of magnitude lower ($\log D(m^2\,s^{-1}) = -21.61$

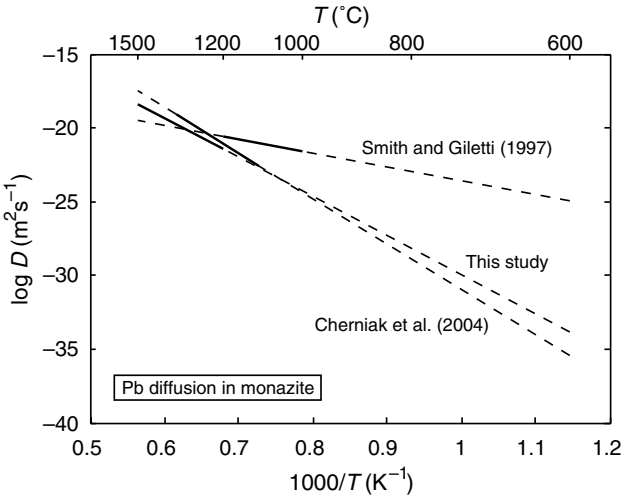

Fig. 8. Experimental measurements of Pb diffusion in monazite. The solid lines represent the Arrhenius laws as given by each author. The dashed lines represent extrapolations.

and $\log D(m^2\,s^{-1}) = -20.59$). At 1100 and 1000 °C the difference between the extrapolation of our versus their diffusivities increases to about three orders magnitude at 1000 °C ($\log D(m^2\,s^{-1}) = -24.30$ and $\log D(m^2\,s^{-1}) = -21.57$). This significant discrepancy is not fully understood, but we must stress some differences between our experiments and those of Smith and Giletti (1997). First of all, we used synthetic crystals whereas they used natural ones. Cherniak et al. (2004) made experiments on both synthetic and natural crystals but did not observe significant differences. The anisotropy measured by Smith and Giletti (1997) is weak and cannot explain the three orders magnitude difference between their data and ours at 1000 °C. Another possibility could be a change in the diffusion mechanism around 1200 °C, yielding to a break in the diffusion coefficient slope. However, the difference between the diffusivities at this temperature is significant and Cherniak et al. (2004) did not observe any break in slope around 1200 °C although their experiments overlapped this temperature. Thus the discrepancy between our data and those of Smith and Giletti (1997) may come from analytical biases, as suggested by Cherniak et al. (2004).

For the temperatures common to Cherniak et al. (2004) (i.e., 1200, 1250, 1300, and 1350 °C), our average diffusivities have less than one order of magnitude difference. Both extrapolations have also less than one order of magnitude difference in the 750–1500 °C range. This very good agreement is surprising since the two experimental protocols are quite different. Indeed, in our experiments Pb diffusion is coupled to that of Th but Th is absent from the Cherniak et al. (2004) experiments using synthetic crystals. Even if those authors do not mention coupling in their experiments, this would suggest that Pb is the limiting species in our experiments and that the diffusion law we obtained could be representative of Pb tracer diffusivity in monazite.

4.3. Quantification of Pb loss via diffusion

All the calculations and conclusions of this section are based on the extrapolation to lower temperatures of the diffusion law established in the present study.

4.3.1. Pb loss under isothermal conditions

We estimated the total Pb loss of monazite via diffusion during a thermal event with the following assumptions: (1) the event is isothermal. Note that non-isothermal histories can be reduced to isothermal ones (e.g., Lasaga, 1983; Chakraborty and Ganguly, 1991); (2) the Pb concentration in the grain is initially uniform. The analytical solution for any initial concentration profile can be found in Crank (1975); (3) the surface concentration is fixed to zero. Even if this does not represent the natural case, this is the condition for which the loss will be the greatest; (4) the production of radiogenic Pb is negligible during the event. This is a reasonable assumption for monazite since ^{232}Th, ^{235}U and ^{238}U half-lives are ~14 Ga, ~0.7 Ga, and ~4.5 Ga, respectively; (5) diffusion is isotropic; and (6) the grain is spherical. The analytical solutions for other geometries can be found in Crank (1975). With these assumptions, the total amount of Pb, M_t, leaving the grain after time t is given by Crank (1975, p. 91, eq. 6.20):

$$\frac{M_t}{M_\infty} = 1 - \frac{6}{\pi^2}\sum_{n=1}^{\infty}\frac{1}{n^2}\exp\left(\frac{-Dn^2\pi^2 t}{a^2}\right), \tag{2}$$

where M_∞ is the initial amount of Pb and a the grain radius. Fig. 9 shows the calculated total Pb losses for three grain sizes, as a function of temperature and time. Total resetting of a monazite via diffusion can only occur at high temperatures and for long metamorphic events. For instance, a 50 μm grain loses 99% of Pb at 900 °C in ~1 Ga. As the time necessary to reset (at the 99% level) a 10 μm grain at 800 °C is longer than the age of the Earth, we conclude that 800 °C is a minimum temperature to reset U–Th–Pb systems via diffusion for most monazite grains. The effect of grain size is very important. Eq. 2 implies that, for a given temperature and a given loss, the duration is proportional to a^2. For instance, at 900 °C, the time necessary to reach 99% loss is ~40 Ma for a 10 μm grain and ~9 Ga for a 150 μm grain.

Partial resetting also requires high temperatures and long metamorphic events: a 50 μm grain loses 1% Pb at 700 °C in ~900 Ma. As the time necessary to lose 1% Pb for a 10 μm grain at 600 °C is longer than the age of the Earth, we consider that below 600 °C most of monazite crystals should remain closed with respect to diffusion. It should be noted that for a given temperature the duration needed to start the reset is much shorter than the time needed to achieve it. For instance, a 50 μm grain heated at 800 °C loses 1% Pb in ~3 Ma but needs durations longer than the age of the Earth to be reset at the 99% level.

One may be interested to know if the core of a grain retained the crystallisation age after a thermal event. The concentration at the center of the grain after time t, C_t, is given by Crank (1975, p. 91, eq. 6.19):

$$\frac{C_\infty - C_t}{C_\infty} = 1 + 2\sum_{n=1}^{\infty}(-1)^n\exp\left(\frac{-Dn^2\pi^2 t}{a^2}\right), \tag{3}$$

where C_∞ is the initial concentration and a the grain radius. Fig. 10 reports the temperatures and the time durations needed to decrease the core concentration by 1% for three grain sizes. The time necessary to lose 1% Pb at the center of a 50 μm grain at 800 °C is longer than the age of the Earth, and this is true at 750 °C for a 10 μm grain. Therefore, most of crystals that did not experience a temperature of more than 750 °C should preserve old ages in their core, if only diffusion is considered to operate as the resetting mechanism.

4.3.2. Closure temperatures

The concept of closure temperature has been introduced by Dodson (1973), and recently extended by Ganguly and Tirone (1999), in order to interpret the apparent ages of

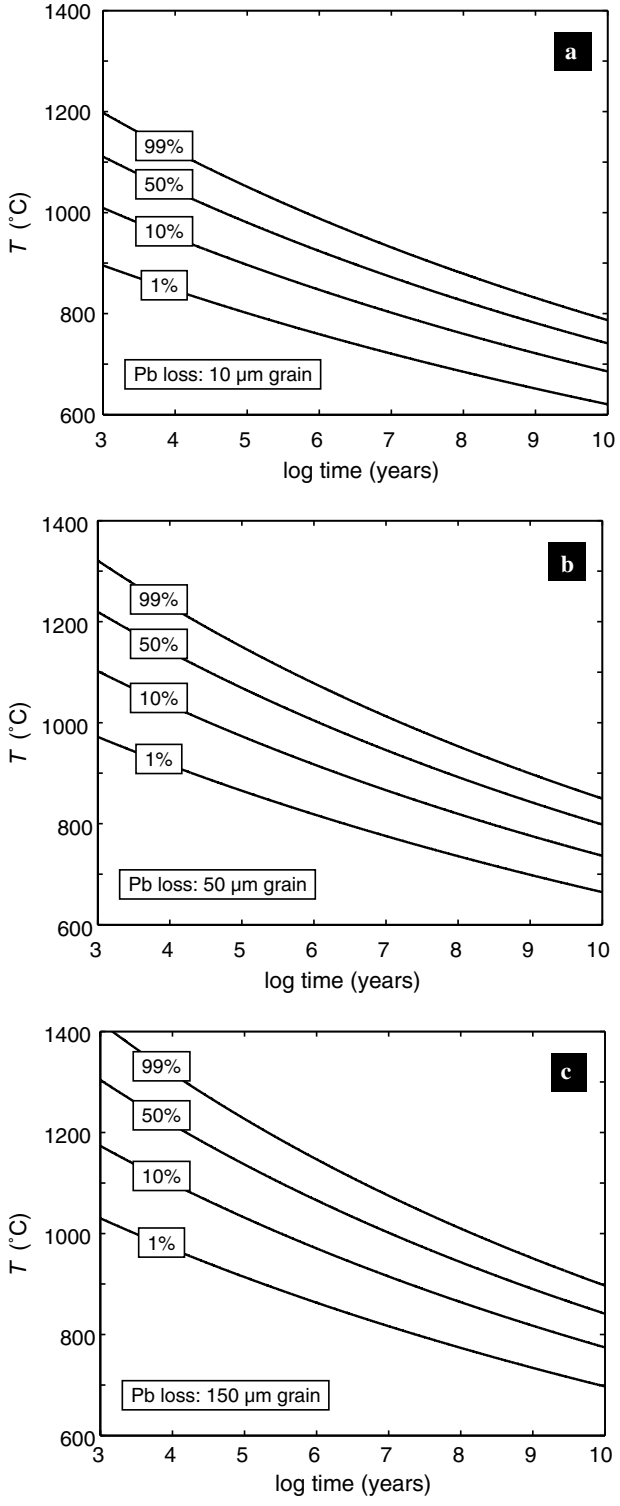

Fig. 9. Temperature–time maps of Pb loss via diffusion in (a) 10, (b) 50, and (c) 150 μm monazite grains. See Section 4.3.1 for details.

minerals that lose radiogenic elements by diffusion during thermal events and subsequent coolings. A set of precise conditions is necessary to apply the closure temperature concept. The most important condition is that the mineral must be completely lacking the daughter product before cooling. If this condition is not fulfilled the concept of

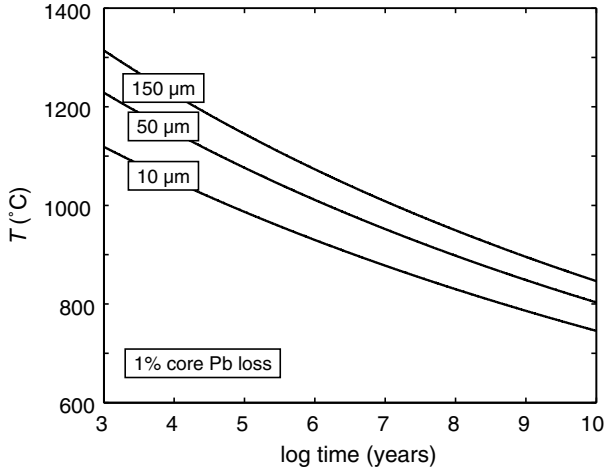

Fig. 10. Temperature–time conditions for 1% Pb loss at the center of 10, 50, and 150 μm monazite grains via diffusion. See Section 4.3.1 for details.

closure temperature is meaningless. Thus, given the results of Section 4.3.1, the closure temperature concept is not applicable for most monazite grains (i.e., greater than 10 μm) which did not experience temperatures above 800 °C. Fig. 11 reports calculated closure temperatures T_c from Dodson's (1973) formulation:

$$\frac{E}{RT_c} = \ln\left(\frac{ART_c^2 D_0/a^2}{E\mathrm{d}T/\mathrm{d}t}\right), \quad (4)$$

where $\mathrm{d}T/\mathrm{d}t$ is the cooling rate (taken to be positive), $A = 55$ (spherical grain), a the grain radius, and R the gas constant. Closure temperatures are always above 800 °C for grains greater than 10 μm and cooling rates greater than 0.1 °C/Ma. For a 50 μm grain and a cooling rate of 1 °C/Ma, the closure temperature is about 900 °C. Hence, the applicability of closure temperature is limited to very high temperature events, and is therefore irrelevant most of the time for U–Th–Pb geochronological systems in monazite.

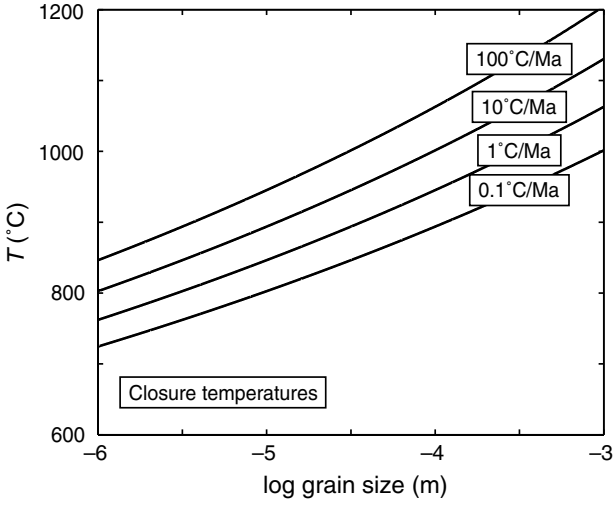

Fig. 11. Closure temperatures for U–Th–Pb systems in monazite in function of grain size and for 0.1, 1, 10, and 100 °C/Ma cooling rates. See Section 4.3.2 for details.

4.4. Natural case

The $Pb^{2+} + Th^{4+} \Longleftrightarrow 2LREE^{3+}$ exchange for Pb diffusion in natural monazite is plausible since Th and LREE are major elements in this mineral. It will be difficult to demonstrate that it occurs in natural samples since (1) Pb concentration is low, and thus the modification of Th distribution due to the co-diffusion with Pb will be low, and (2) this process is very slow and most profiles should be sub-micrometric. However, investigations of such short profiles with low concentrations are possible using ion microprobe and can be used to constrain the thermal history of the mineral (Grove and Harrison, 1999).

Suzuki et al. (1994) reported Pb concentration profiles in metamorphic monazites. These ~20 and ~50 μm profiles were found in two populations of monazites that experienced 620 and 680 °C events respectively. Assuming these profiles were induced by a 5 Ma-long diffusion event, they estimated the diffusivities to be $1.9 \pm 0.3 \times 10^{-25}$ $m^2 s^{-1}$ and $1.5 \pm 0.3 \times 10^{-24}$ $m^2 s^{-1}$ at 620 and 680 °C, respectively. This allowed them to estimate the Arrhenius parameters $\log D_0(m^2 s^{-1}) = -10.47$ (−15.07 to 3.34) and $E = 244$ (118 to 529) kJ mol^{-1}. The experimental data of Smith and Giletti (1997) are in good agreement with these estimates, but the results of the present study and Cherniak et al. (2004) predict diffusion coefficients about 7–9 orders of magnitude lower over the same temperature range. The results of Suzuki et al. (1994) appear to be unique, as we are unaware of any other reports of such long (>10 μm) Pb diffusion profiles in natural monazites.

Indeed, the general case is that monazite that experienced metamorphic events (up to granulites facies) displays homogeneous age distribution or more or less complex discrete age domains with sharp boundaries (e.g., DeWolf et al., 1993; Bingen and van Breemen, 1998; Braun et al., 1998; Cocherie et al., 1998; Crowley and Ghent, 1999; Zhu and O'Nions, 1999; Seydoux-Guillaume et al., 2003; Paquette et al., 2004). Such features favor a low diffusivity of Pb in monazite, in agreement with our study and that of Cherniak et al. (2004).

We therefore conclude that Pb diffusion is not an efficient mechanism to disturb the U–Th–Pb systems. Moreover the complex age domain distributions observed for numerous discordant monazites and the efficiency of experimental resetting of monazite under hydrothermal conditions (Teufel and Heinrich, 1997; Seydoux-Guillaume et al., 2002) suggest U–Th–Pb systems disturbances are mainly due to dissolution–precipitation.

5. Conclusions

1. We measured the Pb diffusivity for $Pb^{2+} + Th^{4+} \Longleftrightarrow 2Nd^{3+}$ interdiffusion from $Nd_{0.66}Pb_{0.17}Th_{0.17}PO_4$ thin films into $NdPO_4$ crystals normal to (−1 0 1) using TEM and RBS. The Arrhenius parameters are:

$$\log D_0(m^2 s^{-1}) = -3.41 \pm 0.77,$$

$$E = 509 \pm 24 \text{ kJ mol}^{-1}.$$

2. $Pb^{2+} + Th^{4+} \Longleftrightarrow 2LREE^{3+}$ interdiffusion is plausible for Pb diffusion in natural monazite since Th and LREE are major elements in this mineral.
3. The extrapolation of the Arrhenius law to crustal temperatures yields very low Pb diffusivities. Grains greater than 10 μm have to experience temperatures above 800 °C to be completely reset, whatever the duration. As the closure temperature can be used only if the grains have been completely reset before cooling, this concept is not suitable for U–Th–Pb systems in monazite.
4. The measurements of the present study are not consistent with Smith and Giletti (1997) but are in agreement with Cherniak et al. (2004). This concordance may suggest that Pb is the limiting species in $Pb^{2+} + Th^{4+} \Longleftrightarrow 2Nd^{3+}$ interdiffusion and thus that our measurements represent the Pb tracer diffusivity in $NdPO_4$.
5. Evidences from the literature of Pb retention of monazite during metamorphic events (up to granulites facies) are in agreement with our results: Pb diffusion is not an efficient mechanism to disturb the U–Th–Pb ages of monazites at common crustal temperatures. The perturbations most probably result from interactions with fluid phases.

Acknowledgments

We thank I. Vickridge, C. Cohen, and all the SAFIR staff at the INS-Paris for their reliable comments and technical support for RBS analysis. We greatly benefited from discussions with F. Béjina on numerous points of this study. Thanks are due to P. de Parseval for his helpful assistance with electron microprobe analysis. Reviews of D.J. Cherniak, J. Brenan, and two anonymous reviewers significantly improved the manuscript.

Associate editor: Yuri Amelin

References

Bingen, B., van Breemen, O., 1998. U–Pb monazite ages in amphibolite- to granulite-facies orthogneiss reflect hydrous mineral breakdown reactions: Sveconorwegian Province of SW Norway. *Contrib. Mineral. Petrol.* **132**, 336–353.

Boatner, L.A., 2002. Synthesis, structure and properties of monazite, pretulite, and xenotime. In: *Phosphates: Geochemical, Geobiological and Materials Importance*. In: Hughes, J.M., Kohn, M., Rakovan, J. (Eds.), *Reviews in Mineralogy and Geochemistry*, vol. 48. Mineralogical Society of America, pp. 87–121.

Braun, I., Montel, J.M., Nicollet, C., 1998. Electron microprobe dating of monazites from high-grade gneisses and pegmatites of the Kerala Khondalite Belt, southern India. *Chem. Geol.* **146**, 65–85.

Chakraborty, S., Ganguly, J., 1991. Compositional zoning and cation diffusion in garnets. In: Ganguly, J. (Ed.), *Diffusion, Atomic ordering and mass transport*, *Advances in Physical Geochemistry*, 8. Springer-Verlag, pp. 198–220.

Cherniak, D.J., Watson, E.B., Grove, M., Harrison, T.M., 2004. Pb diffusion in monazite: a combined RBS/SIMS study. *Geochim. Cosmochim. Acta* **68**, 829–840.

Cocherie, A., Legendre, O., Peucat, J.J., Kouamelan, A.N., 1998. Geochronology of polygenetic monazites constrained by in situ electron microprobe Th–U-total lead determination: Implications for lead behavior in monazite. *Geochim. Cosmochim. Acta* **62**, 2475–2497.

Cohen, C., 1972. Phénomènes de canalisation. *Bull. Soc. Fr. Minéral. Cristallogr.* **95**, 670–683.

Crank, J., 1975. *The mathematics of diffusion*, second ed. Oxford University Press.

Crowley, J.L., Ghent, E.D., 1999. An electron microprobe study of the U–Th–Pb systematics of metamorphosed monazite: the role of Pb diffusion versus overgrowth and recrystallization. *Chem. Geol.* **157**, 285–302.

Dahl, P.S., 1997. A crystal-chemical basis for Pb retention and fission-track annealing systematics in U-bearing minerals, with implications for geochronology. *Earth Planet. Sci. Lett.* **150**, 277–290.

DeWolf, C.P., Belshaw, N., O'Nions, R.K., 1993. A metamorphic history from micron-scale $^{207}Pb/^{206}Pb$ chronometry of Archean monazite. *Earth Planet. Sci. Lett.* **120**, 207–220.

Dodson, M.H., 1973. Closure temperature in cooling geochronological and petrological systems. *Contrib. Mineral. Petrol.* **40**, 259–274.

Donovan, J.J., Hanchar, J.M., Picolli, P.M., Schrier, M.D., Boatner, L.A., Jarosewich, E., 2003. A re-examination of the rare-earth-element orthophosphate standards in use for electron-microprobe analysis. *Can. Mineral.* **41**, 221–232.

Doolittle, L.R., 1985. Algorithms for the rapid simulation of Rutherford backscattering spectra. *Nucl. Instr. Meth. Phys. Res.* **9**, 344–351.

Doolittle, L.R., 1986. A semiautomatic algorithm for Rutherford backscattering analysis. *Nucl. Instr. Meth. Phys. Res.* **15**, 227–231.

Dowty, E., 1980. Crystal-chemical factors affecting the mobility of ions in minerals. *Am. Mineral.* **65**, 174–182.

Feldman, L.C., Mayer, J.W., 1986. *Fundamentals of surface and thin film analysis*. Elsevier, North Holland.

Ganguly, J., Tirone, M., 1999. Diffusion closure temperature and age of a mineral with arbitrary extent of diffusion: theoritical formulation and applications. *Earth Planet. Sci. Lett.* **170**, 131–140.

Grove, M., Harrison, T.M., 1999. Monazite Th–Pb age depth profiling. *Geology* **27**, 487–490.

Harrison, T.M., Catlos, E.J., Montel, J.M., 2002. U–Th–Pb dating of phosphates minerals. In: Hughes, J.M., Kohn, M., Rakovan, J. (Eds.), *Phosphates: Geochemical, Geobiological and Materials Importance*, *Reviews in Mineralogy and Geochemistry*, vol. 48. Mineralogical Society of America, pp. 523–558.

Jaoul, O., Sautter, V., Abel, F., 1991. Nuclear microanalysis: a powerful tool for measuring low atomic diffusivity with mineralogical applications. In: Ganguly, J. (Ed.), *Diffusion, Atomic ordering and mass transport*, *Advances in Physical Geochemistry*, vol. 8. Springer-Verlag, pp. 198–220.

Lasaga, A.C., 1983. Geospeedometry: an extension of geothermometry. In: Saxena, S.K. (Ed.), *Kinetics and Equilibrium in Mineral Reactions*, *Advances in Physical Geochemistry*, vol. 3. Springer-Verlag, pp. 81–114.

L'Hoir, A., Schmaus, D., Cawley, J., Jaoul, O., 1981. Depth profiling light nuclei in single crystals: a combined nuclear reaction and RBS technique to minimize unwanted channeling effects. *Nucl. Instr. Meth.* **191**, 357–366.

Meldrum, A., Boatner, L.A., Weber, W.J., Ewing, R.C., 1998. Radiation damage in zircon and monazite. *Geochim. Cosmochim. Acta* **62**, 2509–2520.

Montel, J.M., Devidal, J.L., Avignant, D., 2002. X-ray diffraction study of brabantite–monazite solid solutions. *Chem. Geol.* **191**, 89–104.

Ni, Y., Hughes, J.M., Mariano, A.N., 1995. Crystal chemistry of the monazite and xenotime structures. *Am. Mineral.* **80**, 21–26.

Overwijk, M.H.E., van den Heuvel, F.C., Bulle-Lieuwma, C.W.T., 1993. Novel scheme for the preparation of transmission electron microscopy specimens with a focused ion beam. *J. Vacuum Sci. Technol.* **11**, 2021–2024.

Paquette, J.L., Goncalves, P., Devouard, B., Nicollet, C., 2004. Micro-drilling ID-TIMS U–Pb dating of single monazites: a new method to unravel complex poly-metamorphic evolutions. Application to the UHT granulites of Andriamena (North-Central Madagascar). *Contrib. Mineral. Petrol.* **147**, 110–122.

Parrish, R.R., 1990. U–Pb dating of monazite and its application to geological problems. *Can. J. Earth Sci.* **27**, 1431–1450.

Roberts, S., McCaffrey, J., Giannuzzi, L., Stevie, F., Zaluzec, N., 2001. Advances techniques in TEM specimen preparation. In: Zhang, X.F., Zhang, Z. (Eds.), *Progress in Transmission Electron Microscopy*, *Springer Series in Surface Sciences*, vol. 38, pp. 336–342.

Seydoux-Guillaume, A.M., Paquette, J.L., Wiedenbeck, M., Montel, J.M., Heinrich, W., 2002. Experimental resetting of the U–Th–Pb systems in monazite. *Chem. Geol.* **191**, 165–181.

Seydoux-Guillaume, A.M., Goncalves, P., Wirth, R., Deutsch, A., 2003. Transmission electron study of polyphase and discordant monazite: site-specific specimen preparation using the focused ion beam technique. *Geology* **31**, 973–976.

Seydoux-Guillaume, A.M., Wirth, R., Deutsch, A., Schärer, U., 2004. Microstructure of 24–1928 Ma concordant monazites; implications for geochronology and nuclear waste deposits. *Geochim. Cosmochim. Acta* **68**, 2517–2527.

Shannon, R.D., 1976. Revised effective ionic radii and systematics studies of interatomic distances in halides and chalcogenides. *Acta Crystallogr.* **A32**, 751–767.

Smith, H.A., Giletti, B.J., 1997. Lead diffusion in monazite. *Geochim. Cosmochim. Acta* **61**, 1047–1055.

Suzuki, K., Adachi, M., Kajizuka, I., 1994. Electron microprobe observations of Pb diffusion in metamorphosed detrital monazites. *Earth Planet. Sci. Lett.* **128**, 391–405.

Teufel, S., Heinrich, W., 1997. Partial resetting of the U–Pb isotope system in monazite through hydrothermal experiments: an SEM and U–Pb isotope study. *Chem. Geol.* **137**, 273–281.

Wirth, R., 2004. Focused ion beam (FIB): a novel technology for advanced application of micro- and nanoanalysis in geosciences and applied mineralogy. *Eur. J. Mineral.* **16**, 863–876.

Young, R.J., 1997. Application of the focused ion beam in materials characterization and failure analysis. *Microstructural Science* **25**, 491–496.

Zhu, X.K., O'Nions, R.K., 1999. Zonation of monazite in metamorphic rocks and its implications for high-temperature thermochronology: a case study from the Lewisian terrain. *Earth Planet. Sci. Lett.* **171**, 209–220.